

Accepted Manuscript

Synthesis, Structural, Theoretical Studies and Biological Activities of 3-(arylamino)-2-phenyl-1*H*-inden-1-one Derivative

Hamdy S. El-Sheshtawy, Ahmed M. Abou Baker

PII: S0022-2860(14)00310-X

DOI: <http://dx.doi.org/10.1016/j.molstruc.2014.03.042>

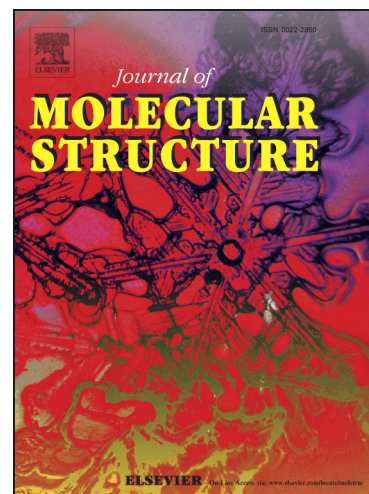
Reference: MOLSTR 20476

To appear in: *Journal of Molecular Structure*

Received Date: 7 November 2013

Revised Date: 13 March 2014

Accepted Date: 14 March 2014



Please cite this article as: H.S. El-Sheshtawy, A.M. Abou Baker, Synthesis, Structural, Theoretical Studies and Biological Activities of 3-(arylamino)-2-phenyl-1*H*-inden-1-one Derivative, *Journal of Molecular Structure* (2014), doi: <http://dx.doi.org/10.1016/j.molstruc.2014.03.042>

This is a PDF file of an unedited manuscript that has been accepted for publication. As a service to our customers we are providing this early version of the manuscript. The manuscript will undergo copyediting, typesetting, and review of the resulting proof before it is published in its final form. Please note that during the production process errors may be discovered which could affect the content, and all legal disclaimers that apply to the journal pertain.

Synthesis, Structural, Theoretical Studies and Biological Activities of 3-(arylamino)-2-phenyl-1*H*-indene-1-one Derivative

Hamdy S. El-Sheshtawy^{a*}, and Ahmed M. Abou Baker^a

^aChemistry Department, Faculty of Science, South Valley University, 83523 Qena, Egypt

Abstract

Five derivatives of 2-phenyl-1*H*-indene-1-one have been prepared and fully characterized. Spectroscopic techniques such as FT-IR, ¹H-NMR, mass spectrometry, and elemental analysis were used to investigate the chemical structures and physical properties of the prepared compounds. The optimized structures and the distribution of the frontier molecular orbital were obtained using density functional theory (DFT) at B3LYP/6-311++G(d,p) level of theory. Additionally, the UV spectral properties of the indene compounds were corroborated by frontier orbital (HOMO and LUMO) calculations. Intramolecular charge transfer (ICT) peak has been observed in the UV spectra of the compounds and theoretically confirmed by the HOMO and LUMO analysis. The potential use of these compounds as antibacterial agents was investigated. The results show that indene-1-one derivatives have an antibacterial activity for both gram-negative (*Pseudomonas aeruginosa*) and gram-positive (*Methicillin Resistant Staphylococcus aureus*) bacteria.

Keywords: 3-(arylamino)-2-phenyl-1*H*-inden-1-one, spectral properties, DFT calculations, biological activities.

^a*Corresponding author:

Tel.: +201062668020,

Fax: +2096-5211279

E-mail: h.elsheshtawy@sci.svu.edu.eg

1. Introduction

Indene compounds have recently attracted the interest of researchers as important intermediates for the synthesis of a wide range of chemicals such as polymers, liquid crystals and enzyme inhibitors [1-6]. In particular, metal complexes of indene derivatives have shown an exceptional catalytic efficiency in the polymerization of ethylene and propylene (Ziegler-Natta type catalysis). Furthermore, indene derivatives have been widely used as cancer inhibition drugs, pesticides and antimicrobial agents [7, 8]. Remarkably, 2-phenyl-1*H*-inden-1-one has been well known as anticoagulant and vitamin K antagonist [9, 10]. Therefore, efficient synthetic pathways to indene derivatives are in high demand. The second position is particularly reactive and indan-1,3-dione derivatives with unique chemical and physical properties [11, 12] may be obtained by functionalizing the methylene bridge [11-13]. The photophysical properties of the derivatives obtained are mainly due to the strong electron-accepting ketone moieties that may couple with electron-donating substituents such as phenyl [11]. On the other hand, addition reactions on the carbonyl groups of 2-phenyl-indan-1,3-dione in the literature is scarce [14].

Donor-acceptor (D-A) molecules have been intensively explored for their potential use as efficient electroluminescent and nonlinear optical materials [15-18]. In this context, the efficiency largely depends on the optimum choice of a good donor-acceptor pair and the proper spacing group. Most of the previously reported materials were based on conjugated polymers [19-21]. Only recently, small molecules with intramolecular charge transfer (ICT) are being investigated for their potential use as nonlinear optics materials [22-24].

In this work five derivatives of 3-(arylamino)-2-phenyl-1*H*-inden-1-one have been synthesized and characterized with spectroscopic techniques such as FT-IR, ¹H-NMR, mass spectrometry and elemental analysis for their possible use as electroluminescent and nonlinear optical materials. Quantum chemical calculations were performed using density-functional theory (DFT) at B3LYP/6-311++G(d,p) level of theory for more insight on the electronic structure and the confirmations of the compounds. The UV-Vis spectroscopic studies, along with the highest occupied molecular orbital (HOMO) and the lowest unoccupied molecular orbital (LUMO) analysis have been used to explain the ICT phenomena within these molecules. In addition, the potential use of the studied compounds as antibacterial agents was investigated.

2. Experimental

2.1 Materials, measurements, and calculations

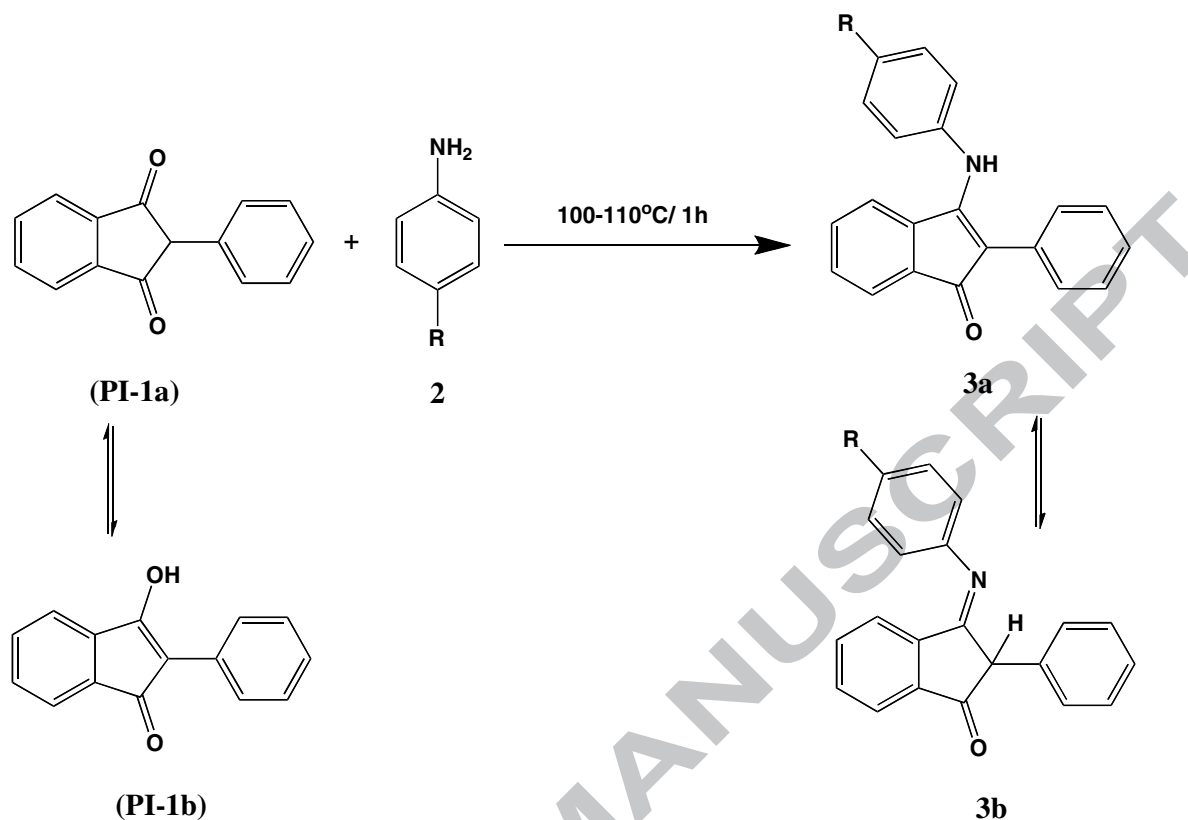
All chemicals and reagents used for the synthesis were purchased from Merck KGaA, Darmstadt, Germany, and used without further purification. Melting points (uncorrected) were recorded on a Griffin & George melting point apparatus. The UV-vis absorption spectra were recorded on a UV-2401PC "UV-VIS Recording Spectrophotometer". The ¹H-NMR spectra were recorded on a Varian Mercury-300BB "NMR300" spectrometer using a TMS internal reference. Electron impact mass spectra were obtained at 70 eV electron impact

ionization energy, using a GCMS sp.1000 Shimadzu. Infrared spectra were recorded with KBr disks on a Bruker Tensor Model spectrophotometer. The FT-IR spectra were recorded from 500 to 4500 cm^{-1} . The average of 8 scans were used at a resolution of 4 cm^{-1} , and the KBr disks were prepared by standard procedures. Elemental analyses were carried out at the Microanalytical unit at Cairo University, Egypt.

All the calculations were performed by the Gaussian03 program [25]. Ground state geometries were calculated using Kohn-Sham density-functional theory (DFT) with the Becke3-Lee-Yang-Parr hybrid functional (B3LYP) method using the 6-311++G(d,p) basis set [26] for the full structural optimization and frequency calculations. Analytical frequency calculations were done in order to verify the stationary points on the potential energy surface. Exclusively positive frequencies and no imaginary negative frequencies for the energy minima were found. To calculate excitation energies, the time-dependant density functional theory (TD-DFT) were also conducted at the B3LYP/6-311++G(d,p) level of theory.

2.2 General synthetic method for the 3-(arylamino)-2-phenyl-1H-inden-1-one derivatives (PHI, PMI, PMOI, PCI, and PNI).

A mixture of 2-phenyl-indan-1,3-dione **PI** (**1a**, **1b**; 2.2 mg; 10 mmol), prepared according to literature,[27, 28] and the corresponding primary aromatic amines **2** (10 mmol), namely, aniline, *p*-toluidine, *p*-anisidine, *p*-chloroaniline and *p*-nitroaniline, was fused at 100-110 $^{\circ}\text{C}$ for 1 h and left stirring overnight. The condensation of **PI** with the different aromatic amines proceeded via a nucleophilic attack of the amines followed by elimination of one water molecule [29]. The solid compounds obtained were filtered and recrystallized from the appropriate solvent to give **PHI**, **PMI**, **PMOI**, **PCI**, and **PNI**, respectively (**3a** and **3b**, in Scheme 1).



R = H (**PHI**), CH₃ (**PMI**), OCH₃ (**PMOI**), Cl (**PCI**), NO₂ (**PNI**)

Scheme 1. The synthetic route of 3-(arylamino)-2-phenyl-1H-inden-1-one.

2.3 Characterization of the 3-(arylamino)-2-phenyl-1H-inden-1-one derivatives (**PHI**, **PMI**, **PMOI**, **PCI**, and **PNI**)

The **PHI** compound was obtained in 86% yield after recrystallization from chloroform. The *m.p.* was 168–170 °C and ¹H-NMR (DMSO): δ = 6.87–7.73 (m, 14H, arom. H), 9.87 (s, 1H, NH); IR (KBr, cm⁻¹): 3235 (NH), 3053, 2890 (CH₂), 1657 (C=O), 1592 (C=N), 1120 (C-N); MS: *m/z* = 297 (100%) (M⁺); Anal. Calcd. for C₂₁H₁₅NO. C, 84.82; H, 5.08; N, 4.71. Found; C, 84.55; H, 5.13; N, 4.94 %.

The **PMI** compound was obtained in 90% yield after recrystallization from ethanol, m.p 232-234 °C; $^1\text{H-NMR}$ (DMSO): $\delta = 2.15$ (s, 3H, CH_3), 6.83-7.72 (m, 13H, arom. H), 9.84 (s, 1H, NH); IR (KBr, cm^{-1}): 3232 (NH), 3050, 2887 (CH_3 , CH_2), 1659 (C=O), 1589 (C=N), 1122 (C-N); MS: $m/z = 311$ (99.7%) (M^+); *Anal.* Calcd. For $\text{C}_{22}\text{H}_{17}\text{NO}$. C, 84.86; H, 5.50; N, 4.50. Found; C, 84.69; H, 5.45; N, 4.72 %.

The **PMOI** compound was obtained in 93% yield after recrystallization from chloroform. M.p. 226-228 °C and $^1\text{H-NMR}$ (DMSO): $\delta = 3.62$ (s, 3H, OCH_3), 6.55-7.64 (m, 13H, arom. H), 9.79 (s, 1H, NH); IR (KBr, cm^{-1}): 3235 (NH), 3055, 2887 (CH_3O , and CH_2), 1661 (C=O), 1594 (C=N), 1124 (C-N); MS: $m/z = 327$ (25.7%) (M^+); *Anal.* Calcd. For $\text{C}_{22}\text{H}_{17}\text{NO}_2$. C, 80.71; H, 5.23; N, 4.28. Found; C, 84.84; H, 5.36; N, 4.03 %.

The **PCI** compound was obtained in 88% yield after recrystallization from chloroform/ethanol (3:1). M.p. 244-246 °C; $^1\text{H-NMR}$ (DMSO): $\delta = 6.88$ -7.76 (m, 13H, arom. H), 9.92 (s, 1H, NH); IR (KBr, cm^{-1}): 3240 (NH), 3054, 2879 (CH_2), 1662 (C=O), 1609 (C=N), 1120 (C-N); MS: $m/z = 331$ (67.3%) (M^+); *Anal.* Calcd. For $\text{C}_{21}\text{H}_{14}\text{NOCl}$. C, 76.02; H, 4.25; N, 4.22; Cl, 10.69. Found; C, 76.10; H, 4.32; N, 4.19; Cl, 10.57 %.

The **PNI** compound was obtained in 94% yield after recrystallization from ethanol, m.p 272-274 °C; $^1\text{H-NMR}$ (DMSO): $\delta = 7.07$ -7.82 (m, 13H, arom. H), 10.29 (s, 1H, NH); IR (KBr, cm^{-1}): 3257 (NH), 3055, 2878 (CH_2), 1666 (C=O), 1610 (C=N), 1093 (C-N); MS: $m/z = 342$ (42.4%) (M^+); *Anal.* Calcd. For $\text{C}_{21}\text{H}_{14}\text{N}_2\text{O}_3$. C, 73.68; H, 4.12; N, 8.18. Found; C, 73.54; H, 4.09; N, 8.35 %.

2.4 Antibacterial activity test

An *in vitro* antibacterial and antifungal activity assay was performed by the paper disc assay method using the agar nutrient as medium. The 3-(arylamino)-2-phenyl-1*H*-inden-1-one were tested against gram positive and negative bacteria (*Pseudomonas aeruginosa*, *Methicillin-Resistant Staphylococcus aureus*). The stock solutions were prepared by dissolving the compounds in ethanol and the solutions were serially diluted in order to find the minimum inhibitory concentration values (MIC). All the blank discs were moistened with the solvent. For disc assays, Chloramphenicol-treated strains were used as a positive control. The diameters of the growth inhibition hollows caused by samples were measured and expressed in millimeter. All the assays were carried out in triplicate.

3. Results and Discussion

3.1 Molecular structures and geometry optimization

The **PI** compound was synthesized by the reaction of phthalic anhydride and phenylacetic acid according to literature [28, 30, 31]. Calculations with density functional theory (DFT) at the B3LYP/6-311++G(d,p) level of theory [26] show that the keto-form (**PI-1a**) exists in equilibrium with the enol-form (**PI-1b**) and is 3.77 kcal mol⁻¹ more stable, in the gas phase [31, 32]. This result is in a good agreement with the X-ray structure reported by Bravic *et al.* [33], who showed that **PI** exists in organic solvents in keto–enol tautomerism but only in its keto-form in the crystal structure [32, 33]. The phenyl ring in the keto-form (**1a**) is not in the same plane with the indan-1,3-dione moiety, but rather at a torsional angle C1–C2–C3–C4 of 90° and 75° (Fig. 1), in the X-ray structure and in the gas phase calculations, respectively [32, 33]. In the enol-form (**1b**), the phenyl ring is only slightly deviated from

planarity, with a C1-C2-C3-C4 torsional angle of approximately 143° (Fig. 1), allowing an unfavorable OH...H (2.16 Å) interaction and a C=O...H interaction of a favorable distance of 2.60 Å, but an unsuitable bond angle of 110.4° [34-36], which may account for the instability of this form compared to the keto-form.

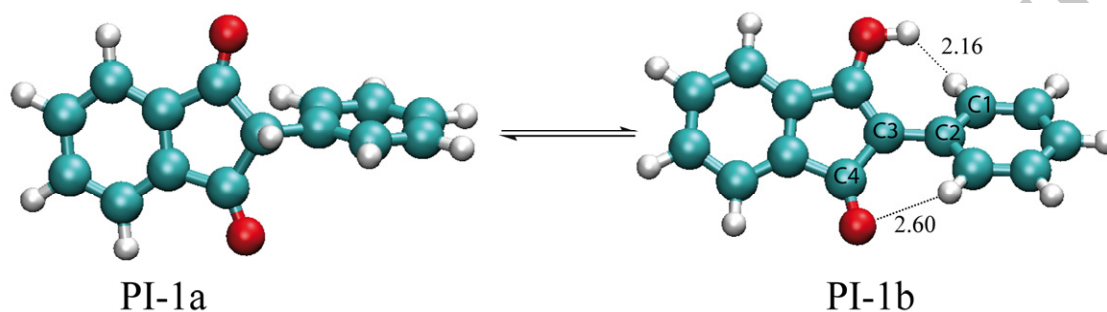


Fig. 1. Optimized molecular structure of the **PI-1a** and **PI-1b** isomers calculated at B3LYP/6-311++G(d,p) level of theory.

The optimized structures and DFT calculated energies with B3LYP/6-311++G(d,p) level show that the amide form **3a** exists in equilibrium with the imide form **3b**. The **3a** isomer is approximately 4 kcal/mol more stable than **3b** (see Table 1, and S1-S10 Supplementary data). Interestingly, the geometrical structure of **3a** has the phenyl ring twisted from the indan moiety plane; the dihedral angle (C1-C2-C3-C4) is, for example, 140.5° in case of **PHI-3a**, and 58.2° for **PHI-3b** (Fig. 2 and Table 1). The steric repulsion between the hydrogen atom of the indane benzene ring and the phenyl ring may be held responsible for the lower stability displayed by the amide isomer **3b** [34, 37]. The stability of the possible conformation isomers of **3a** was explored particularly around the C5-N1 bond. For example, the potential energy surface of **PHI** shows stabilization of **PHI-3a** by 2.3 kcal, the dihedral angle C8-C5-N1-H1 = 160° , than the corresponding isomer where C8-C5-N1-H1 = 0° (see Fig. S5, Supplementary data).

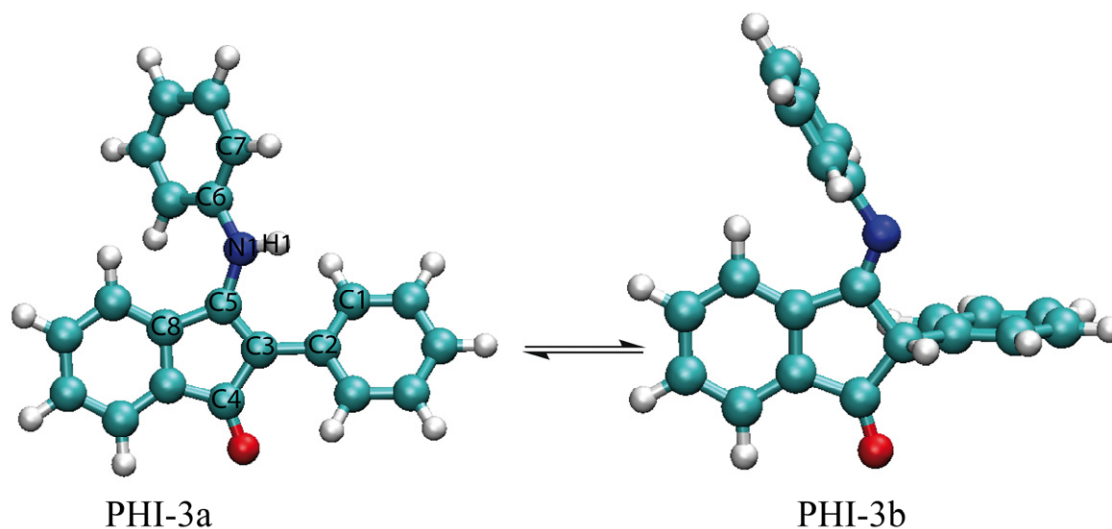


Fig. 2. Molecular structure of **PHI-3a** and **PHI-3b** isomers calculated at B3LYP/6-311++G(d,p) level of theory.

3.2 Vibrational spectra

Experimental FT-IR corroborated with theoretical calculations (DFT) reveals the presence of an amide-imide tautomerism. The calculated and experimental FT-IR spectra of the most stable isomers of **3** are shown in Fig. 3, and Fig. S1-S4, Supplementary data. Selected vibrational modes are collected in Table 2. For example, the FT-IR spectra of **PHI** show N-H stretching frequencies of 3235 cm^{-1} , 1530 cm^{-1} (C=C), as well as $1566\text{--}1594\text{ cm}^{-1}$ stretching vibrations, corresponding to C=N stretching, as it is usually the case for amide-imide tautomers [38-40]. Simulated FT-IR spectra, scaled by a factor of 0.963 [41], support the experimental results and show the difference between **3a** and **3b** isomers. Again, the vibrational peaks at 3563 cm^{-1} (N-H), and the peak at 1600 cm^{-1} C=N, and 1414 cm^{-1} sp^2 (C=C) are well resolved in the **3a** compounds. Their absence in the **3b** compounds supports tautomerism equilibrium. In addition, C=O stretching peak in the region $1800\text{--}1680\text{ cm}^{-1}$

was observed for the all compounds which its position depends on the group environment [38, 42, 43].

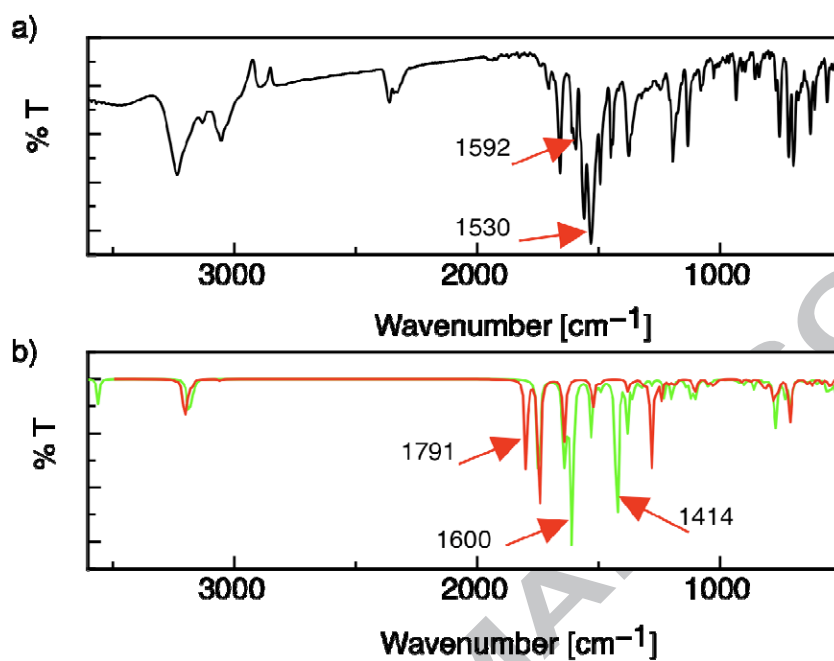


Fig. 3. a) Experimental FT-IR of **PHI**, b) calculated vibrational absorption spectra of **PHI**, **3a** (green) and **PHI**, **3b** (red), at the optimized structure by B3LYP/6-311++G(d,p) level of theory.

Table 1: Optimized bond lengths (Å), bond angles (°), dihedral angles (°) and stabilization energy, include zero point energy corrections, (kcal/ mol) of 3-(arylamino)-2-phenyl-1H-inden-1-one derivatives obtained by B3LYP/6-311++G(d,p) level of theory.

		PHI		PMI		PMOI		PCI		PNI	
		3a	3b								
Dihedral angles	C1-C2-C3-C4	140.5	58.2	140.5	68.3	140.2	58.7	140.3	60.9	140.7	59
	C1-C2-C3-C5	-39.9	-61	-40.1	-50.9	-40.3	-61.5	-40.0	-58.7	-39.4	-60.6
	C5-N1-C6-C7	154.4	-88.7	150.8	-94.5	146.2	-76.1	155.5	-92.1	165.3	-90.7
Bond angles	C2-C3-C5	127.8	114.7	127.7	115	127.7	115	127.8	114.7	128.8	126.3
	C5-N1-C6	128.4	124.3	128.1	124.1	127.6	124	128	124.5	128.1	114.7
Bond lengths	C5-N1	1.37	1.27	1.37	1.27	1.42	1.28	1.37	1.26	1.38	1.27
	C6-N1	1.41	1.41	1.42	1.41	1.42	1.41	1.41	1.40	1.40	1.39
ΔE		-4.58	-	-4.82	-	-4.25	-	-4.10	-	-3.43	-

Table 2: Experimental and calculated [B3LYP/6-311++G(d,p)] [26] vibrational frequencies (ν cm⁻¹) of 2-phenyl-1*H*-indene-1-one derivatives.

Compound	Experimental	Calculated		assignment
		a	b	
PHI	3235	3435		ν (N-H)
	3053	3076	3093	ν (C-H)ph
	2890			ν (C-H)alph
	2824			ν (C-H)alph
	1705		1742	ν (C=N)
	1657	1696	1684	ν (C=O)
	1592	1593	1584	ν (C=O)
	1558	1558	1473	ν (CC)ph, ν (C=N)
	1530		1414	ν (C=C)
	1492	1379	1341	δ (N-H)
	1449	1336	1238	δ (C-H)ph
PMI	3232	3440	3097	ν (N-H)
	3050	3071		ν (C-H)ph
			3040	ν (CH ₃)as
	2887	2999		ν (C-H)alph, ν (CH ₃)
	2360	2969		ν (C=N)
			1743	ν (C=O)
	1657	1683	1683	ν (C=O)
	1589	1589	1593	ν (CC)ph, ν (C=N)
	1533		1400	ν (C=C)
	1490	1495		δ (CC)ph
	1440	1431	1288	δ (N-H)
PMOI	3235	3116		ν (N-H)
	3055		3050	ν (C-H)ph
	2887	2937	2972	ν (C-H)alph, ν (CH ₃)
	2360	2728	2913	ν (C-H)alph, ν (CH ₃)
		2275		ν (C-H)alph, ν (CH ₃)
			1747	ν (C=N)
	1661	1646	1679	ν (C=O)
	1594	1595	1593	ν (C=O)
	1562	1533		ν (CC)ph
	1532	1499	1499	ν (C=N)
	1465	1472	1465	ν (C=C)
1439	1446	1293	δ (CC)ph	
1419	1429	1241	δ (N-H)	
PCI	3240	3431		ν (N-H)
	3054	3079	3093	ν (C-H)ph
	2879			ν (C-H)alph
	2360			ν (C-H)alph
			1742	ν (C=N)
	1662	1691		ν (C=O)
	1609	1589	1683	ν (C=O)
	1587	1563	1588	ν (CC)ph, ν (C=N)
	1560		1420	ν (C=C)
	1488	1481	1477	δ (CC)ph
	1403	1379		δ (N-H)

PNI	3257	3409	3093	$\nu(\text{N-H})$
	2878	3084		$\nu(\text{C-H})_{\text{alph}}$
	2359			$\nu(\text{C-H})_{\text{alph}}$
			1742	$\nu(\text{C-H})_{\text{alph}}$
	1666	1705	1700	$\nu(\text{C=N})$
	1610	1589	1588	$\nu(\text{C=O})$
	1566	1525	1525	$\nu(\text{CC})_{\text{ph}}, \nu(\text{C=N})$
	1540		1420	$\nu(\text{C=C})$
	1488	1481	1472	$\delta(\text{CC})_{\text{ph}}$
	1375	1365		$\delta(\text{N-H})$

^a Calculated vibrational signals were scaled by 0.963 [41].

3.3 UV-Vis absorption spectra

The UV-Vis absorption spectra of **PHI**, **PMI**, **PMOI**, **PCI**, and **PNI** were measured in ethanol and are shown in Fig. 4. The recorded absorption spectra show characteristic peaks at 250–300 nm, a shoulder at ca. 310 nm, and broad peak at 400–550 nm (Table 3). The 272–276 nm peaks are characteristic for a local $\pi\pi^*$ electronic transition and the maxima at 450–454 nm pertains to the ground state intramolecular charge transfer (ICT) between the arylamino donor and the 2-phenyl-1*H*-inden-1-one acceptor group (*vide infra*). In addition, the 309 nm shoulder is due to the equilibrium between the amide and imide tautomers (Scheme 1). Interestingly, **PNI** shows an extra peak at 351 nm.

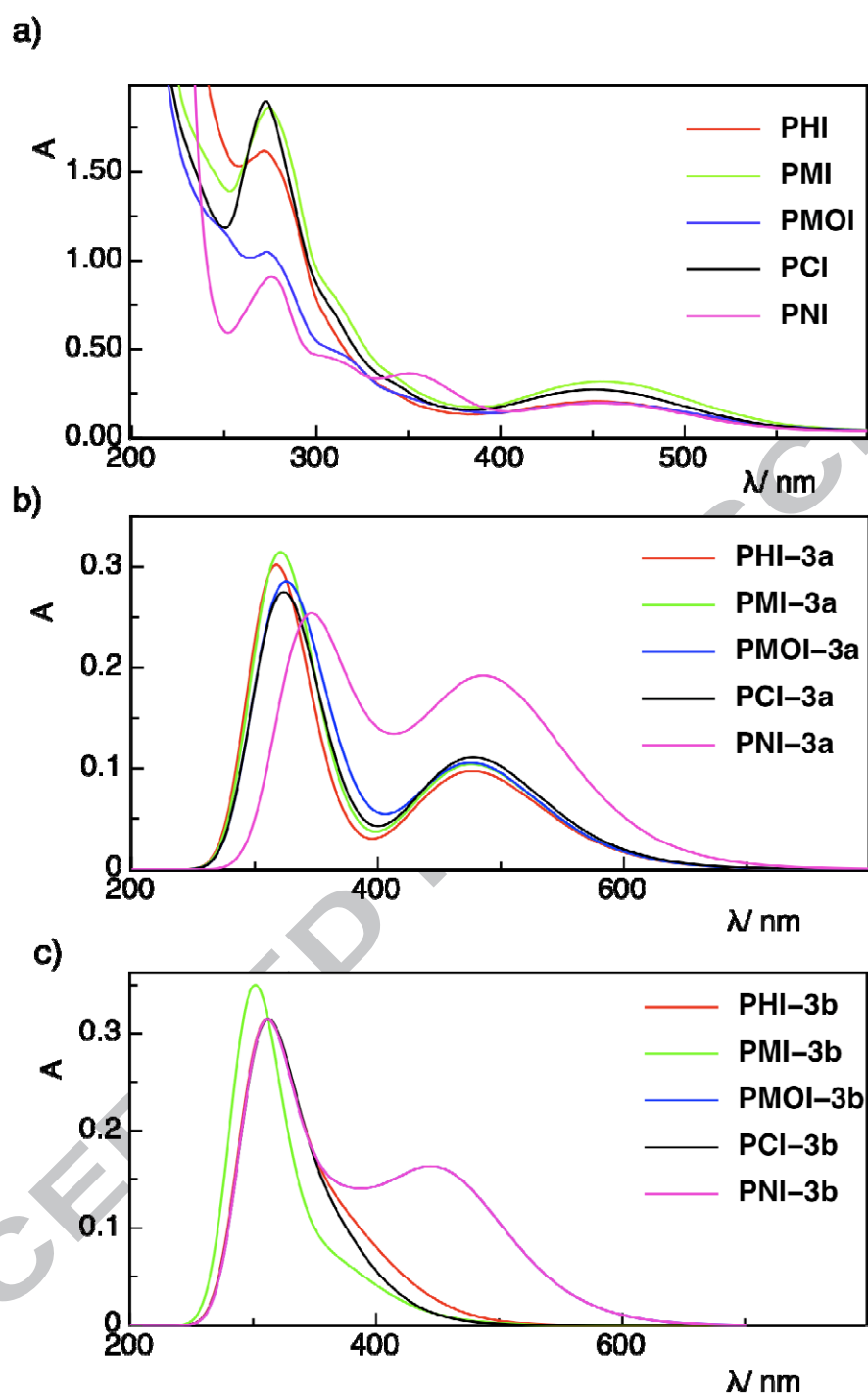


Fig. 4: a) Absorption spectra of **3** in ethanol (3.4 μM PHI; 5.1 μM PMI; 2.6 μM PMOI; 4.0 μM PCI; 6.0 μM PNI), b) Predicted absorption spectra of **3a**, C) Predicted absorption spectra of **3b** with TD-DFT at B3LYP/6-311++G(d,p) level of theory.

3.4 Frontier orbital (HOMO-LUMO) calculations

In order to understand the experimental *UV-vis* absorption spectra, TD-DFT calculations for **PHI**, **PMI**, **PMOI**, **PCI**, and **PNI** were performed at B3LYP/6-311++G(d,p) level to investigate the nature of both HOMO and LUMO orbitals [44, 45]. The experimental wavelengths, the calculated energy values and the oscillator strengths of the near *UV-vis* spectra are shown in Table 3. The optimized geometries in Fig. 5 for the highest HOMO and the lowest LUMO orbitals reveal that the electron density transfer occurs from the more aromatic part of the π conjugated system (the electron donor) to the electron deficient part (the electron acceptor). The HOMO is distributed over both the aryl group and the indene moiety, while the indene moiety has the largest contribution to the LUMO orbital for both **3a** and **3b** isomers (see Fig. 5 and S6, Supplementary data). Exceptionally, both **PNI** derivative isomers have the larger contribution to the LUMO orbital located on the phenyl ring in addition to the indene moiety (Fig. 5), which may be due to the low energy difference of this particular derivative between its LUMO (3.15 eV) and LUMO+1 (2.64 eV). This result implies that the 2-(nitrophenyl) moiety can work as electron acceptor in addition to the indene moiety. The presence of two acceptors centers and one electron donor site in **PNI-3a** explain the presence of the extra peak of this derivative at 351 nm (Fig. 4).

Table 3: Experimental and predicted wavelength (λ), oscillator strength (f), and excitation energy (eV) of 3-(arylamino)-2-phenyl-1H-inden-1-one derivatives obtained by B3LYP/6-311++G(d,p) level of theory.

	λ (nm)						
	Observed	Predicted		f (a.u)		E (eV)	
		3a	3b	3a	3b	3a	3b
PHI	272	299	300	0.008	0.0007	4.14	4.13
	309 sh	309	367	0.055	0.0022	4.01	4.08
	450	477	408	0.096	0.0008	2.60	3.04
PMI	274	301	298	0.025	0.0110	4.12	4.15
	309 sh	308	372	0.006	0.0060	4.03	4.10
	455	476	423	0.103	0.0004	2.60	2.93
PMOI	274	306	300	0.0059	0.0002	4.05	4.13
	314 sh	307	392	0.0680	0.0021	4.04	4.09
	453	476	457	0.1039	0.0037	2.60	2.71
PCI	272	307	301	0.0781	0.0013	4.03	4.11
	308 sh	312	369	0.0094	0.0030	3.96	4.05
	451	477	411	0.1092	0.0002	2.59	3.01
PNI	276	329	314	0.0170	0.0175	3.76	3.94
	309 sh	331	326	0.0313	0.2044	3.75	3.79
	351	345	384	0.1969	0.0338	3.58	3.79
	454	493	420	0.1782	0.0011	2.51	3.22

The energy gap between the HOMO and LUMO orbitals generally determine the molecular chemical activity, optical polarizability, kinetic stability, bioactivity and chemical hardness of the molecule. Table 4 depicts the HOMO, LUMO, and energy gap values for the **3a** and **3b** isomers. The small energy gap of the studied compounds implies that there is a

small energy barrier to be overcome for electron transfer and substantial ground state internal charge transfer (ICT) occurs, which is experimentally confirmed by a charge transfer band (Fig. 4). The energy gap values (Table 4) are smaller for the amide form (**3a**) than the imide form (**3b**). Therefore, the former is more reactive than the latter isomer. Note that the energy gaps, calculated at the B3LYP/6-311++G(d,p) level of theory, are comparable to energy gaps of other conjugated polymers [46] and small organic molecules [47].

The TD-DFT calculations with simulated electronic transitions of both **3a** and **3b** isomers explain the *UV-vis* absorption spectra observed for these derivatives. The predictions give the electronic absorption spectra for the singlet-singlet transitions (see Fig. 4b and 4c). For the **3a** isomers, intense absorption peaks are simulated in the *UV* region with a strong maximum at 299, 301, 306, 307, and 329 nm (corresponding to the experimental 272–276 nm absorption) and less intensive peaks in the visible range at 477, 476, 476, 478, and 493 nm (corresponding to the ICT experimental peaks at 450–454 nm) for **PHI-3a**, **PMI-3a**, **PMOI-3a**, **PCI-3a**, and **PNI-3a**, respectively. These assignments are based on the predicted high oscillator strength values and low excitation energy values of the corresponding peaks (Table 3). On the other hand, the simulated electronic absorption spectra of the **3b** isomers show intense peaks in the *UV* region (300 – 320 nm) and shoulder peaks in the visible region at 367, 372, 392, 369, and 384 nm for **PHI-3b**, **PMI-3b**, **PMOI-3b**, **PCI-3b**, and **PNI-3b**, respectively. The broad absorption shoulders predicted for the **3b** isomers in the visible region may be corresponding to the shoulders experimentally obtained at 310 nm. In the particular case of **PNI**, the experimental peak observed at 350 nm is present in the simulation of **3b** at 420 nm.

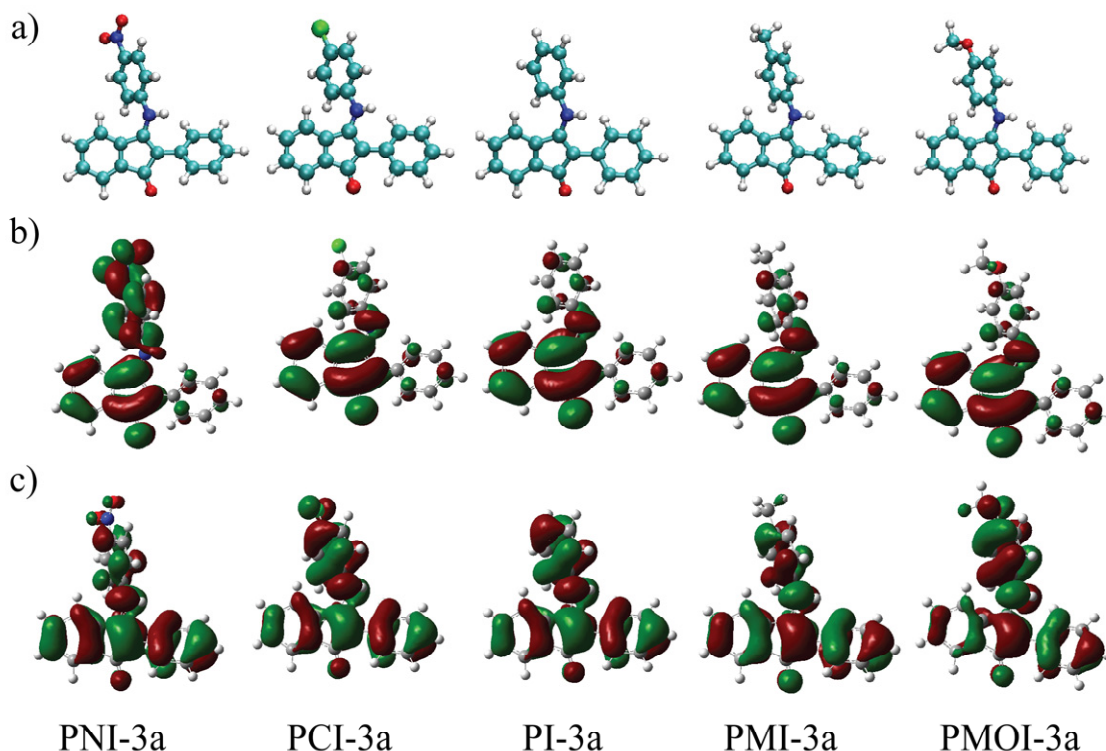


Fig. 5: (a) The optimized structure, (b) lowest unoccupied molecular orbital (LUMO), (c) highest occupied molecular orbital (HOMO) of **PNI-3a**, **PMI-3a**, **PMOI-3a**, **PCI-3a**, and **PNI-3a** isomers calculated at B3LYP/6-311++G(d,p) level of theory.

3.5 The dipole moment

The dipole moment (μ), which results from the non-uniform distribution of charges on the different atoms in a molecule, is another important electronic property of molecules. This is mainly used to study the intermolecular interactions (e.g. Van der Waals, dipole-dipole, π - π). The dipole moment is directly proportional to the strength of the intermolecular interaction; the larger the dipole moment, the stronger the intermolecular interactions. Table 4 lists the dipole moment (μ) for both isomers of the 3-(arylamino)-2-phenyl-1H-inden-1-one synthesized derivatives, and shows that the **3a**, amide isomers are always more polar than the **3b** imide, therefore, having a stronger tendency for intermolecular interactions. The only

exception is the **PNI** derivative, which has a lower dipole moment value and, hence, a lower tendency for the intermolecular interactions in its **3a** isomer form.

Table 4: Predicted dipole moment (μ), HOMO and LUMO energies (E_{HOMO} and E_{LUMO}), and the band gap energies (ΔE) of the 3-(arylamino)-2-phenyl-1H-inden-1-one derivatives.

	PHI		PMI		PMOI		PCI		PNI	
	3a	3b								
E_{HOMO} (eV)	-5.69	-6.21	-5.61	-6.03	-5.55	-5.73	-5.81	-6.28	-6.18	-6.87
E_{LUMO} (eV)	-2.49	-2.37	-2.42	-2.33	-2.36	-2.31	-2.62	-2.49	-3.15	-2.76
ΔE (eV)	-3.20	-3.84	-3.19	-3.70	-3.19	-3.42	-3.19	-3.79	-3.03	-4.11
μ (D)	4.97	3.61	3.02	2.33	5.94	4.42	3.06	2.33	3.35	4.29

3.6 Molecular electrostatic potential (MEP) surface

The molecular electrostatic potential (MEP) surface has been intensively used for the investigation of the chemical reactivity of the molecules [48]. This is usually investigated by generating an electrostatic potential $V(r)$ in the space around the molecule and predicting the charge distribution. The negative region in MEP is the preferred site for an electrophilic attack while the positive region is the preferred site for a nucleophilic attack. The MEP is further used to predict the active sites in biological systems and, therefore, it is effectively used in biological systems recognition [49]. To predict the electrophilic and nucleophilic reactive sites for both isomers of the 3-(arylamino)-2-phenyl-1H-inden-1-one derivatives, the

MEP was calculated for the optimized structures with B3LYP/6-311++G(d,p) level of theory (Fig. 6). The negative charge densities (red color) are localized on the carbonyl oxygen atoms for both the isomers. The nitrogen atoms of the **3a** isomers bear positive charge densities (blue color), while those of the **3b** isomers have negative charge densities. The nitro group carry a negative charge that is higher in isomer **3a**, as shown by the higher dipole moment of this isomer compared to **3b** (Table 4).

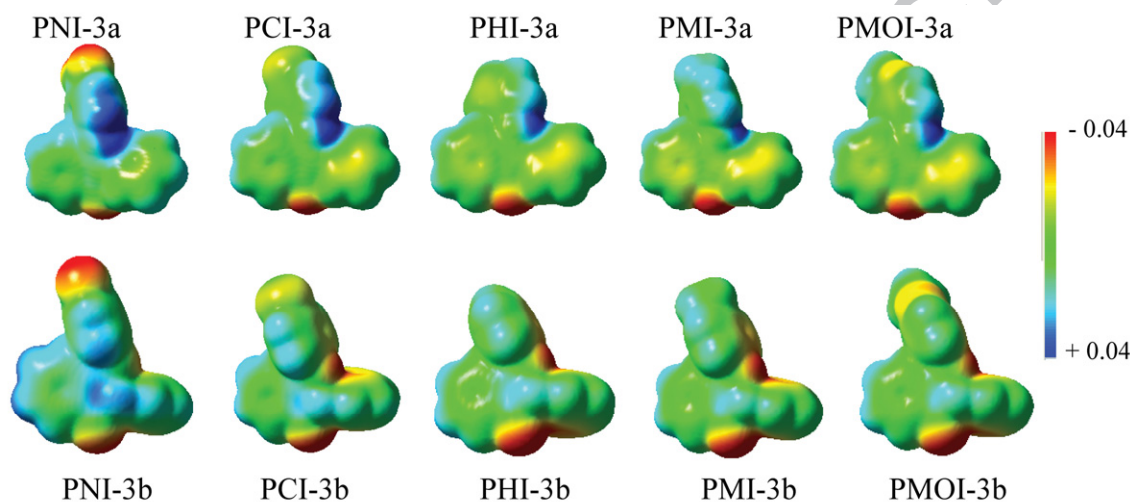


Fig. 6: The MEP surface of 3-(arylamino)-2-phenyl-1H-inden-1-one derivatives calculated at B3LYP/6-311++G(d,p) level of theory (negative charge areas as colored in red, while the positive charged ones are blue).

3.7 Biological activity

The search for new antibiotics is increasing due to the microbes mutations [50, 51]. *Staphylococcus aureus* and *Pseudomonas aeruginosa* are of particular interest due to their versatile pathogenic response, causing a wide range of human diseases such as pustules [52, 53] carbuncles [54] furuncles [55] and impetigo [56]. In addition, *Staphylococcus aureus* is a

well-known infectious agent in hospitals, particularly for new born babies, diabetes patients and chronic diseases [57]. The discovery of penicillin in the early 1940s has reduced the infectiousness of *Staphylococcus aureus* until the penicillin resistant *Staphylococcus aureus* (PRSA) was reported. Methicillin was then discovered as being effective against PRSA infections in the late 1950s, however, only until the Methicillin-Resistant *Staphylococcus aureus* (MRSA) emerged, the treatment of PRSA and MRSA is largely restricted to β lactam antibiotics, although, recently the MRSA becomes resistant to it [58, 59]. Herein, we investigated indene-1-one derivatives for their potential use as medicinal agents for both gram positive and gram-negative bacteria. These compounds were screened for antibacterial activities using Chloramphenicol as reference-antibiotic [60]. The **PHI**, **PCI**, **PMOI** and **PNI** derivatives were biologically active against *Pseudomonas aeruginosa* (Table 5), with **PNI** having the largest effect (14.0 mm) and **PHI** the lowest, compared to the reference antibiotic. The antibacterial trend is in agreement with the increasing inductive effect of the substituted groups (H < -Cl < -OCH₃ < -NO₂) of these derivatives. The derivative, with an electron-donating group (-CH₃), however, does not show any effect on *Pseudomonas aeruginosa*. Interestingly, only **PNI** shows a significant activity against MRSA (15.2 mm). This may be related to the presence of multiple sites for the intermolecular interaction of **PNI**, as the MEP surface shows (Fig. 6). Note that both **PNI** and the reference antibiotic (Chloramphenicol) have the resonance effect of (-NO₂), which may be the link to their similar effect on MRSA.

Table 5: The antibacterial activity of 3-(arylamino)-2-phenyl-1H-inden-1-one derivatives against *Pseudomonas aeruginosa* (ATCC 278223 Gram negative) and *Methicillin Resistant Staphylococcus aureus* (MRSA, ATCC 43300 Gram positive).

	Antibacterial activity (mm)	
	MRSA	<i>Pseudomonas aeruginosa</i>
Chloramphenicol ^a	32.9	21.5
PMOI	–	12.0
PMI	–	–
PHI	–	6.0
PCI	–	10
PNI	15.2	14.0

^aChloramphenicol was used as reference antibiotic.

4. Conclusion

Five derivatives of 3-(arylamino)-2-phenyl-1H-inden-1-one derivatives, **PHI**, **PMI**, **PMOI**, **PCI**, and **PNI**, were synthesized and fully characterized by various analytical techniques. We discussed the presence of amide –imide tautomerism both by experimental and theoretical methods. TD-DFT calculations proved the intramolecular charge transfer (ICT) in these molecules and determined the energy gap between the HOMO and LUMO that allow such ICT processes. Except for the *p*-methyl derivative, all others show an antibacterial effect against *Pseudomonas aeruginosa*, the largest being that of the *p*-nitro derivative. The

structural and spectroscopic properties of the *p*-nitro substituent may be the underlying reason for this unique antibacterial effect on the MRSA.

Acknowledgment

The authors thank the central laboratory at South Valley University for providing the chemical analysis instruments. H. S. El-Sheshtawy thanks the Computational Laboratory for Analysis, Modeling, and Visualization (CLAMV) at the Jacobs University Bremen (Germany) for computation time.

References

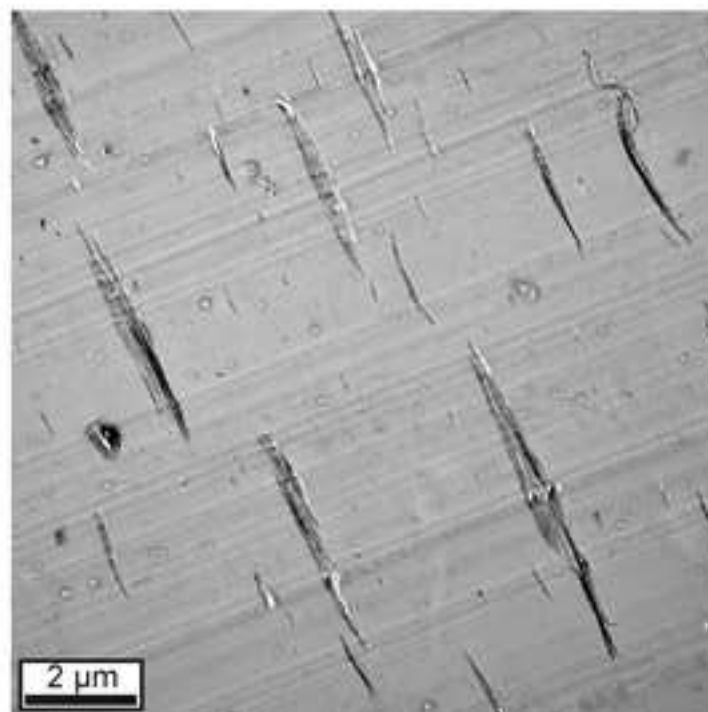
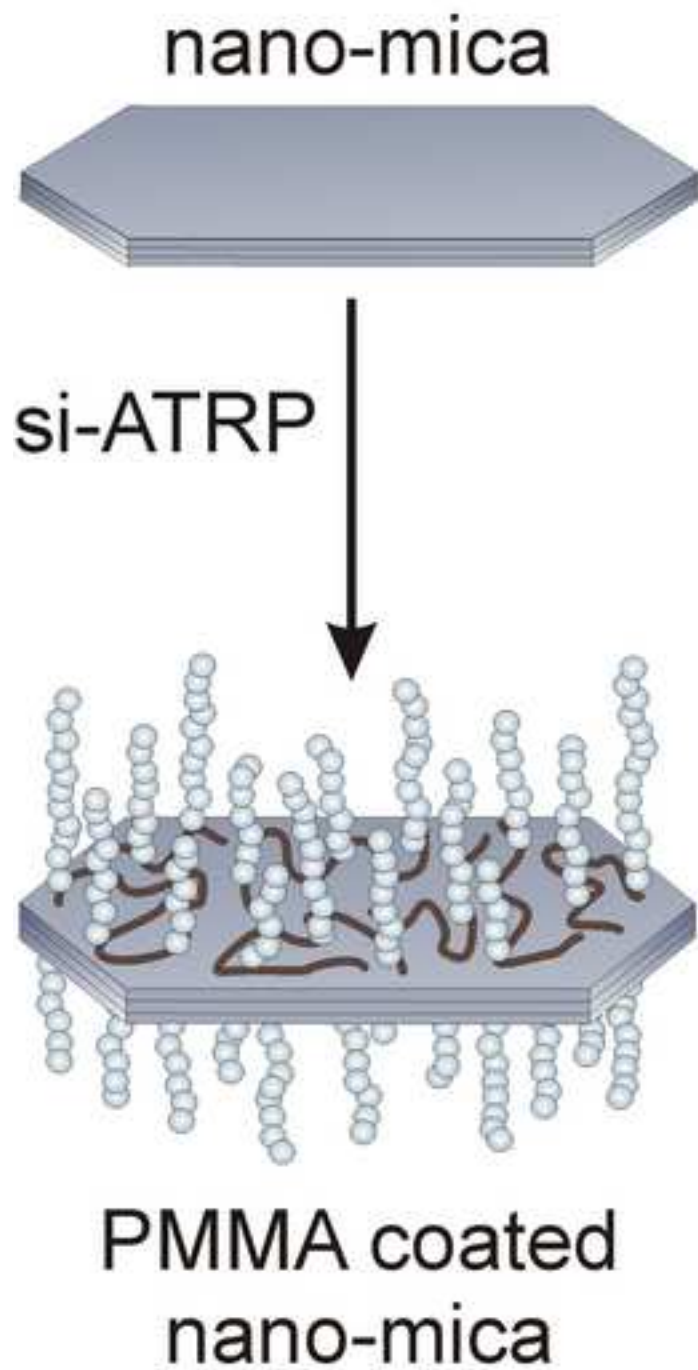
- [1] H.-Y. Chen, S. Lan, P.-C. Yang, S.-H. Lin, J.-Y. Sun, C.-F. Lin, Sol. Energ. Mat. Solar C., 113 (2013) 90-95.
- [2] Y. Sun, C. Cui, H. Wang, Y. Li, Adv. Energy Mater., 2 (2012) 966-969.
- [3] O. Yokokoji, K. Shimizu, S. Inoue, Liq. Cryst., 36 (2009) 1-6.
- [4] S. Basurto, S. Garcia, A.G. Neo, T. Torroba, C.F. Marcos, D. Miguel, J. Barbera, M.B. Ros, M.R. de la Fuente, Chem-Eur. J., 11 (2005) 5362-5376.
- [5] K.E. Peterson, M.A. Cinelli, A.E. Morrell, A. Mehta, T.S. Dexheimer, K. Agama, S. Antony, Y. Pommier, M. Cushman, J. Med. Chem., 54 (2011) 4937-4953.
- [6] A.M. Palmer, S. Christmann, G. Muench, C. Brehm, P.J. Zimmermann, W. Buhr, J. Senn-Bilfinger, M.P. Feth, W.A. Simon, Bioorgan. Med. Chem., 17 (2009) 368-384.
- [7] H. Wong, M. Belvin, S. Herter, K.P. Hoeflich, L.J. Murray, L. Wong, E.F. Choo, J. Pharmacol. Exp. Ther., 329 (2009) 360-367.
- [8] O. Müller, E. Gourzoulidou, M. Carpintero, I.-M. Karaguni, A. Langerak, C. Herrmann, T. Möröy, L. Klein-Hitpaß, H. Waldmann, Angew. Chem. Int. Edit., 43 (2004) 450-454.
- [9] D.J. Naisbitt, J. Farrell, P.J. Chamberlain, J.E. Hopkins, N.G. Berry, M. Pirmohamed, B.K. Park, J. Pharmacol. Exp. Ther., 313 (2005) 1058-1065.

- [10] M. Walis, R. Autor, *Nurs. Stand.*, 15 (2001) 47-54.
- [11] M. Utinans, O. Neilands, *Adv. Mat. Optics Electronics*, 9 (1999) 19-25.
- [12] S. Jursenas, A. Gruodis, G. Kodis, M. Chachisvilis, V. Gulbinas, E.A. Silinsh, *J. Phys. Chem. B*, 102 (1998) 1086-1094.
- [13] A. Ahmedova, V. Atanasov, P. Marinova, N. Stoyanov, M. Mitewa, *Cent. Eur. J. Chem.*, 7 (2009) 429-438.
- [14] V. Enchev, G. Ivanova, G. Pavlovic, M. Rogojerov, A. Ahmedova, M. Mitewa, *J. Mol. Struct.*, 654 (2003) 11-20.
- [15] K.R. Justin Thomas, J.T. Lin, M. Velusamy, Y.T. Tao, C.H. Chuen, *Adv. Funct. Mater.*, 14 (2004) 83-90.
- [16] H.-F. Xiang, Z.-X. Xu, V.A.L. Roy, B.-P. Yan, S.-C. Chan, C.-M. Che, P.T. Lai, *Appl. Phys. Lett.*, 92 (2008) 163305-163303.
- [17] J.C. Collings, S.-Y. Poon, C. Le Droumaguet, M. Charlot, C. Katan, L.-O. Pålsson, A. Beeby, J.A. Mosely, H.M. Kaiser, D. Kaufmann, W.-Y. Wong, M. Blanchard-Desce, T.B. Marder, *Chem-Eur. J.*, 15 (2009) 198-208.
- [18] V.F. Pais, H.S. El-Sheshtawy, R. Fernandez, J.M. Lassaletta, A. Ros, U. Pischel, *E-J. Chem.*, 19 (2013) 6650-6661.
- [19] T. Michinobu, K. Okoshi, H. Sako, H. Kumazawa, K. Shige, *Polymer*, 49 (2008) 192-199.
- [20] H. Yi, R.G. Johnson, A. Iraqi, D. Mohamad, R. Royce, D.G. Lidzey, *Macromol. Rapid Comm.*, 29 (2008) 1804-1809.
- [21] S.M. Shivashankar, V.K. Anantapadmanabha, A.V. Adhikari, *Polym. Eng. Sci.*, 53 (2013) 1347-1356.
- [22] B. Leonardo De, S.C. Daniel, R.M. Cleber, *Nonlinear Optical Absorption of Organic Molecules for Applications in Optical Devices*, InTech, 2010.

- [23] J. Xu, S. Semin, D. Niedzialek, P.H.J. Kouwer, E. Fron, E. Coutino, M. Savoini, Y. Li, J. Hofkens, H. Uji-I, D. Beljonne, T. Rasing, A.E. Rowan, *Adv. Mater.*, 25 (2013) 2084-2089.
- [24] J. M. Cole, Z.F. Weng, *Adv. Mat. Res.*, 123-125 (2010) 959.
- [25] M. J. Frisch, G. W. Trucks, H. B. Schlegel, G. E. Scuseria, M. A. Robb, J. R. Cheeseman, J. A. Montgomery, K.N.K. T. V. Jr., J. C. Burant, J. M. Millam, S. S. Iyengar, J. Tomasi, V. Barone, B. Mennucci, M. Cossi, G. Scalmani, N. Rega, G. A. Petersson, H. Nakatsuji, M. Hada, M. Ehara, K. Toyota, R. Fukuda, J. Hasegawa, M. Ishida, T. Nakajima, Y. Honda, O. Kitao, H. Nakai, M. Klene, X. Li, J. E. Knox, H. P. Hratchian, J. B. Cross, V. Bakken, C. Adamo, J. Jaramillo, R. Gomperts, R. E. Stratmann, O. Yazyev, A. J. Austin, R. Cammi, C. Pomelli, J. W. Ochterski, P. Y. Ayala, K. Morokuma, G. A. Voth, P. Salvador, J. J. Dannenberg, V. G. Zakrzewski, S. Dapprich, A. D. Daniels, M. C. Strain, O. Farkas, D. K. Malick, A. D. Rabuck, K. Raghavachari, J. B. Foresman, J. V. Ortiz, Q. Cui, A. G. Baboul, S. Clifford, J. Cioslowski, B. B. Stefanov, G. Liu, A. Liashenko, P. Piskorz, I. Komaromi, R. L. Martin, D. J. Fox, T. Keith, M. A. Al-Laham, C. Y. Peng, A. Nanayakkara, M. Challacombe, P. M. W. Gill, B. Johnson, W. Chen, M. W. Wong, C. Gonzalez, J. A. Pople, *Gaussian 03 Revision E.01*.
- [26] M.J. Frisch, M. Headgordon, J.A. Pople, *Chem. Phys. Lett.*, 166 (1990) 281-289.
- [27] E. During, *Ber. Dtsch. Chem. Ges.*, 38, (1904) 161.
- [28] G. Vanages, V. Oskaja, *Latv. PSR Zinat. Akad. Vestis*, 3 (1961) 67.
- [29] L. Perreux, A. Loupy, F. Volatron, *Tetrahedron*, 58 (2002) 2155-2162.
- [30] D. Giles, M. S. Prakash, K. V. Ramseshu, *E-J. Chem.*, 4 (2007) 428-433.
- [31] W. Stadlbauer, M. Fischer, *J. Heterocyclic Chem.*, 39 (2002) 131-135.
- [32] L.A. Chetkina, V.K. Belsky, *Crystallogr. Rep.*, 53 (2008) 579-607.
- [33] G. Bravic, J. Gaultier, C. Hauw, *Cryst. Struct. Commun.*, 3 (1974) 215-217.
- [34] C.J. Kim, *Bull. Korean Chem. Soc.*, 23 (2002) 330-336.

- [35] A. Ismael, J.A. Paixao, R. Fausto, M.L.S. Cristiano, *J. Mol. Struct.*, 1023 (2012) 128-142.
- [36] P.A. Wood, F.H. Allen, E. Pidcock, *Crystengcomm*, 11 (2009) 1563-1571.
- [37] R.A. Pascal, *Pure and Appl. Chem.*, 65 (1993) 105-110.
- [38] G. Socrates, *Infrared Characteristic Group Frequencies*, John Wiley & Sons, New York, 2000.
- [39] M. Arivazhagan, D.A. Rexalin, *Spectrochim. Acta A*, 107 (2013) 347-358.
- [40] M. Hagar, S.M. Soliman, F. Ibid, E.S.H. El Ashry, *J. Mol. Struct.*, 1049 (2013) 177-188.
- [41] N. Sundaraganesan, S. Ilakiamani, H. Saleem, P.M. Wojciechowski, D. Michalska, *Spectrochim. Acta A*, 61 (2005) 2995-3001.
- [42] N. Prabavathi, A. Nilufer, V. Krishnakumar, *Spectrochim. Acta A*, 114 (2013) 101-113.
- [43] A. Ismael, A. Borba, L. Duarte, B.M. Giuliano, A. Gomez-Zavaglia, M.L.S. Cristiano, *J. Mol. Struct.*, 1025 (2012) 105-116.
- [44] L. Padmaja, C. Ravikumar, D. Sajan, I.H. Joe, V.S. Jayakumar, G.R. Pettit, O.F. Nielsen, *J. Raman Spectrosc.*, 40 (2009) 419-428.
- [45] C. Ravikumar, I.H. Joe, V.S. Jayakumar, *Chem. Phys. Lett.*, 460 (2008) 552-558.
- [46] A. Misra, P. Kumar, R. Srivastava, S.K. Dhawan, M.N. Kamalasanan, S. Chandra, *Indian J. Pure Ap. Phy.*, 43 (2005) 921-925.
- [47] F. Yakuphanoglu, M. Aydin, N. Arsu, M. Sekerci, *Semiconductors*, 38 (2004) 468-471.
- [48] W. Sun, G. Yuan, J. Liu, L. Ma, C. Liu, *Spectrochim. Acta A*, 106 (2013) 275-283.
- [49] S. Gunasekaran, R.A. Balaji, S. Kumaresan, G. Anand, S. Srinivasan, *Can. J. Anal. Sci. Spectrosc.*, 53 (2008) 149-162.
- [50] J. Davies, D. Davies, *Microbiol. Mol. Biol. R.*, 74 (2010) 417-433.
- [51] D.I. Andersson, D. Hughes, *Nat. Rev. Micro.*, 8 (2010) 260-271.

- [52] G. Pouessel, H. Ythier, O. Carpentier, A. Vachée, J. Etienne, B. Catteau, *Pediatr. Dermatol.*, 24 (2007) 401-404.
- [53] Y. Mengesha, M. Bennett, *Am. J. Clin. Dermatol.*, 3 (2002) 389-400.
- [54] Y. Mine, W. Higuchi, K. Taira, I. Nakasone, M. Tateyama, T. Yamamoto, H. Uezato, K. Takahashi, *J. Dermatol.*, 38 (2011) 1167-1171.
- [55] A. Katsambas, T. Lotti, D. Ioannides, *Furuncles and carbuncles*, *European Handbook of Dermatological Treatments*, Springer Berlin Heidelberg, 2003, pp. 173-176.
- [56] S. Koning, A. van Belkum, S. Snijders, W. van Leeuwen, H. Verbrugh, J. Nouwen, M.O. 't Veld, L.W.A. van Suijlekom-Smit, J.C. van der Wouden, C. Verduin, *J. Clin. Microbiol.*, 41 (2003) 3017-3021.
- [57] R.A. Polin, L. Saiman, *NeoReviews*, 4 (2003) e81-e89.
- [58] D. Golemi-Kotra, J.Y. Cha, S.O. Meroueh, S.B. Vakulenko, S. Mobashery, *J. Biol. Chem.*, 278 (2003) 18419-18425.
- [59] L.D. Sabath, *Ann. Intern. Med.*, 97 (1982) 339-344.
- [60] M. Fukuda, H. Ohashi, C. Matsumoto, S. Mishima, Y. Shimomura, *Cornea*, 21 (2002) S86-S89.



Highlights

- Synthesis of 3-(arylamino)-2-phenyl-1H-inden-1-one derivatives.
- Geometric structure and vibrational spectra of the amide-imide forms were analyzed.
- Experimental photophysical properties were compared with the computed values.
- Biological activities on different bacteria were examined.